

Empirical Fourier Decomposition: An Accurate Adaptive Signal Decomposition

Method

Wei Zhou ^{a, b}

Zhongren Feng ^{a, c}

Y.F. Xu ^{b *}

Xiongjiang Wang ^a

Hao Lv ^a

^a School of Civil Engineering and Architecture, Wuhan University of Technology, Wuhan 430070, P.R. China.

^b Department of Mechanical and Materials Engineering, University of Cincinnati, Cincinnati, OH 45221, USA.

^c School of Urban Construction, Wuchang Shouyi University, Wuhan 430064, P.R. China.

* Corresponding author. Cincinnati, OH 45221, USA.

E-mail: xu2yf@uc.edu

Tel: +1-513-556-2755

Abstract

Signal decomposition is an effective tool to assist the identification of modal information in time-domain signals. Two signal decomposition methods, including the empirical wavelet transform (EWT) and Fourier decomposition method (FDM), have been developed based on Fourier theory. However, the EWT can suffer from a mode mixing problem for time-domain signals with closely-spaced modes and decomposition results by FDM can suffer from an inconsistency problem. An accurate adaptive signal decomposition method is proposed to solve the problems in this work; it is called the empirical Fourier decomposition (EFD). The proposed EFD combines the uses of an improved frequency spectrum segmentation technique and an ideal filter bank. The segmentation technique can solve the inconsistency problem by predefining the number of modes in a time-domain signal to be decomposed and filter functions in the ideal filter bank have no transition phases, which can solve the mode mixing problem. Numerical investigations are conducted to study the accuracy of the EFD. It is shown that the EFD can yield accurate and consistent decomposition results for time-domain signals with multiple non-stationary modes and those with closely-spaced modes, compared with decomposition results by the EWT, FDM, variational mode decomposition, and empirical mode decomposition. It is also shown that the EFD can yield accurate time-frequency representation results and has the highest computational efficiency among the compared methods.

Keywords: signal decomposition; empirical Fourier decomposition; empirical wavelet transform; Fourier decomposition method; ideal filter bank

1. Introduction

Signal decomposition is a widely used numerical tool in different fields, such as biomedical signal analysis [1], seismic signal analysis [2], mechanical vibration signal analysis [3,4], and speech enhancement [5]. Time-domain signals that derive from a physical system usually comprise several superposed components, which are referred to as modes [6], and the modes can encompass meaningful frequency-domain information of the signals. Hence, it is crucial to obtain signal decomposition results with high accuracy and efficiency.

In the past few decades, several signal decomposition methods have been developed, and the empirical mode decomposition (EMD) [7] is one of the most significant methods, even though its mathematical understanding is limited and it has some known shortcomings, such as mode mixing [8] and end effects [9]. Improved versions of the EMD have been developed to overcome the shortcomings. The ensemble EMD [10] has been developed by adding white noise with finite amplitudes to alleviate the mode mixing and end effects problems. The complete ensemble EMD [11] was developed to further improve the EMD by adding completeness and a full data-driven number of modes, which are missing in the ensemble EMD. Li et al. presented a time-varying filter technique to solve the mode mixing problem [12]. However, these EMD methods cannot fundamentally solve the mode mixing and end effects problems. The variational mode decomposition (VMD) proposed by Dragomiretskiy et al. [13] is a non-recursive signal decomposition method, which was developed based on a generalization of Wiener filters. However, the VMD can fail for nonstationary time-domain signals with chirp modes that have overlapping frequency ranges. To avoid this failure, McNeill [14] proposed the use of an optimized objective function with constraints on short-time narrow-band modes, and Chen et al. [15] exploited a complete variational framework to generalize the VMD. The empirical wavelet transform (EWT) employs an adaptive wavelet filter bank based on segments of Fourier spectra [16]. The workability of the EWT has been improved in Ref. [17–19] to eliminate its requirement for a high signal-to-noise ratio in a signal to be decomposed. However, transition phases between filter functions in a wavelet filter bank in the EWT can suffer from the mode mixing problem for signals with closely-spaced modes. Besides, the first decomposed mode by the EWT can correspond to a trivial residual, with which the number of segments is not equal to that of decomposed modes. Fourier decomposition method (FDM) [20] is an adaptive non-stationary, non-linear signal decomposition method that can decompose a zero-mean signal into a set of Fourier intrinsic band functions (FIBFs) based on Fourier theory and Hilbert transform. Several limitations of

the FDM have been identified. To obtain a FIBF, two frequency scan techniques were developed. One is called the low-to-high (LTH) technique and the other is high-to-low (HTL) technique. The LTH and HTL techniques recursively estimate upper and lower bounds of FIBFs, respectively. However, decomposition results by the FDM with the two frequency scan techniques, i.e., FDM-HTL and FDM-LTH, can be inconsistent and one cannot determine which decomposition results are correct. Further, the two frequency scan techniques are both iterative and can lead to long computation time for FDM.

In this work, the EWT and the FDM are briefly reviewed. The segmentation technique and construction of a wavelet filter bank of the EWT are described, and the construction of FIBFs and the two frequency scan techniques of the FDM are described. A new adaptive signal decomposition method, called the empirical Fourier decomposition (EFD), is proposed to solve the aforementioned problems of the EWT and FDM. The EFD combines an improved segmentation technique and an ideal filter bank [21]. The improved segmentation technique consists of an adaptive sorting process to yield unique segmentation results, and the ideal filter bank, whose filter functions have no transition phases, facilitates accurate decomposition for signals with closely-spaced modes. Numerical investigations are conducted to study the accuracy of decomposition results by the EFD for two non-stationary time-domain signals and two time-domain signals with closely-spaced modes by comparing with the EMD, VMD, EWT and FDM. In addition, the accuracy of time-frequency representations (TFRs) and computational efficiency of the EFD are compared with those associated with the other methods.

The remnant of the paper is arranged as follows. In Section 2, the EWT and FDM are briefly reviewed. In Section 3, the proposed EFD is described. In Section 4, the numerical investigations are presented. Conclusions and some discussions on future works are presented in Section 5.

2. Reviews of EWT and FDM

2.1 EWT

The EWT employs an adaptive wavelet transform algorithm based on segments of Fourier spectra [16]. The two most important steps of the EWT are: (1) use of an adaptive segmentation technique to divide Fourier spectrum of a signal to be decomposed and (2) construction of a wavelet filter bank [22]. Assume that the Fourier spectrum is defined on a normalized frequency range $[-\pi, \pi]$. The segmentation technique and wavelet filter bank for the spectrum in the frequency range $[0, \pi]$ are described below, and those for the spectrum in

the frequency range $[-\pi, 0]$ can be deduced based on Hermitian symmetry of a Fourier spectrum with a normalized frequency range $[-\pi, \pi]$.

One segmentation technique for the EWT is the local maxima technique [16], in which the frequency spectrum on $[0, \pi]$ is divided into N contiguous segments. Each segment is denoted by $S_n = [\omega_{n-1}, \omega_n]$ with, $n \in [1, N]$, $\omega_0 = 0$ and $\omega_N = \pi$. The first $N-1$ largest local maxima of the Fourier spectrum magnitudes are identified. The frequencies that uniquely correspond to the identified maxima are reindexed in a descending order and denoted by $[\Omega_1, \Omega_2, \dots, \Omega_{N-1}]$ so that $\Omega_1 < \Omega_2 < \dots < \Omega_{N-1}$. The value of ω_n is determined by

$$\omega_n = \frac{\Omega_{n-1} + \Omega_n}{2}, n \in [1, N-1] \quad (1)$$

which concludes the local maxima technique for segmentation. As an alternative to the local maxima technique, the lowest minima technique [23] was developed for the EWT, in which the frequency spectrum division and frequency reindexing procedures, same as those in the local maxima technique, are carried out. Then the minimum of the spectrum magnitude in the frequency range $[\Omega_{n-1}, \Omega_n]$ is identified and the value of ω_n is determined by

$$\omega_n = \arg \min_{\omega} X_n(\omega), n \in [1, N-1] \quad (2)$$

where $X_n(\omega)$ denotes the spectrum magnitudes in $[\Omega_{n-1}, \Omega_n]$ and $\operatorname{argmin}(\cdot)$ denotes argument of the minimum, which concludes the lowest minima technique for segmentation.

The wavelet filter bank consists of the empirical scaling function $\hat{\phi}_1(\omega)$ and a series of empirical wavelet function $\hat{\psi}_n^{\downarrow}(\omega)$:

$$\hat{\phi}_1(\omega) = \begin{cases} 1 & \text{if } |\omega| \leq \omega_1 - \tau_1 \\ \cos \left[\frac{\pi}{2} \beta \left(\frac{1}{2\tau_1} (\tau_1 + |\omega| - \omega_1) \right) \right] & \text{if } \omega_1 - \tau_1 \leq |\omega| \leq \tau_1 + \omega_1 \\ 0 & \text{otherwise} \end{cases} \quad (3)$$

and

$$\hat{\psi}_n^{\downarrow}(\omega) = \begin{cases} 1 & \text{if } \omega_n + \tau_n \leq |\omega| \leq \omega_{n+1} - \tau_{n+1} \\ \cos \left[\frac{\pi}{2} \beta \left(\frac{1}{2\tau_{n+1}} (\tau_{n+1} + |\omega| - \omega_{n+1}) \right) \right] & \text{if } \omega_{n+1} - \tau_{n+1} \leq |\omega| \leq \tau_{n+1} + \omega_{n+1} \\ \sin \left[\frac{\pi}{2} \beta \left(\frac{1}{2\tau_n} (\tau_n + |\omega| - \omega_n) \right) \right] & \text{if } \omega_n - \tau_n \leq |\omega| \leq \tau_n + \omega_n \\ 0 & \text{otherwise} \end{cases} \quad (4)$$

where $\hat{\phi}_1$ denotes Fourier transform of a function, ω denotes the frequency, β is an arbitrary function and τ_n is a parameter that determines the size of the transition phase associated with the n -th and $(n+1)$ -th segments; the transition phase is defined on the frequency range $[\omega_n - \tau_n, \omega_n + \tau_n]$.

One of the most used forms of β with a variable x is [22]:

$$\beta(x) = \begin{cases} 0 & \text{if } x \leq 0 \\ x^4(35 - 84x + 70x^2 - 20x^3) & \text{if } x \in (0, 1) \\ 1 & \text{if } x \geq 1 \end{cases} \quad (5)$$

The parameter τ_n is determined by

$$\tau_n = \gamma \omega_n \quad (6)$$

where γ is a parameter that should be sufficiently small to prevent overlapping between boundaries of non-zero $\hat{\phi}_1(\omega)$ and $\hat{\psi}_n^{\downarrow}(\omega)$. A criterion for an acceptable value of γ is

$$\gamma < \min_n \left(\frac{\omega_{n+1} - \omega_n}{\omega_{n+1} + \omega_n} \right) \quad (7)$$

for all n values, and its value can be determined by

$$\gamma = \left(\frac{R-1}{R} \right) \min_n \left(\frac{\omega_{n+1} - \omega_n}{\omega_{n+1} + \omega_n} \right) \quad (8)$$

where R is the number of discrete data in the signal to be decomposed. The determinations of $\hat{\phi}_1(\omega)$ and $\hat{\psi}_n^{\downarrow}(\omega)$ with τ_n conclude the construction of the wavelet filter bank. Graphical illustrations of $\hat{\phi}_1(\omega)$ and $\hat{\psi}_n^{\downarrow}(\omega)$ are shown in Figs. 1(a) and (b), respectively.

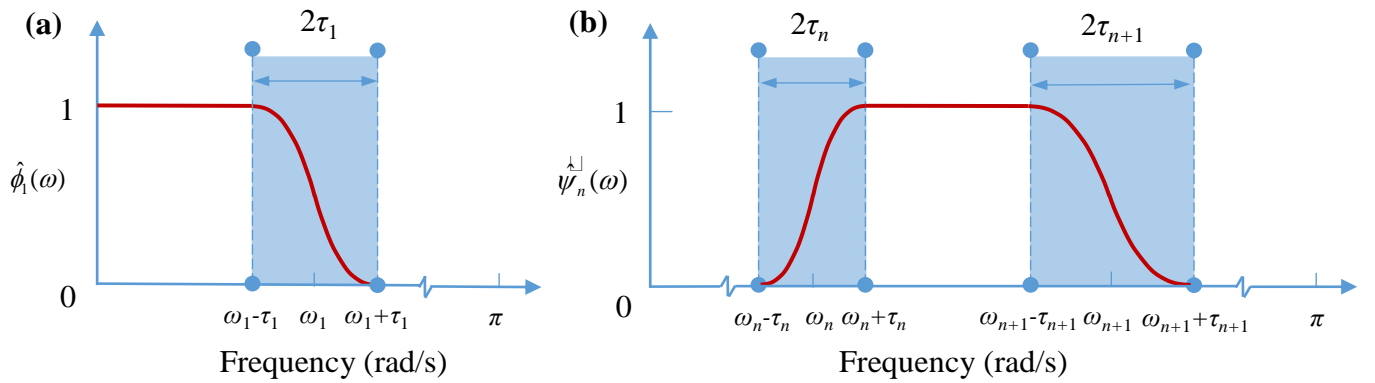


Fig. 1. Graphical illustrations of (a) $\hat{\phi}_1(\omega)$ and (b) $\hat{\psi}_n^{\downarrow}(\omega)$.

After applying the segmentation technique and constructing the filter bank, a signal can be reconstructed as

$$\begin{aligned}\tilde{f}(t) &= f_0(t) + f_1(t) + \dots + f_{N-1}(t) \\ &= W_f^\varepsilon(0, t) * \phi_1(t) + \sum_{n=1}^{N-1} W_f^\varepsilon(n, t) * \psi_n(t)\end{aligned}\quad (9)$$

where the asterisk * denotes the convolution of two functions, $W_f^\varepsilon(0, t)$ and $W_f^\varepsilon(n, t)$ are called the approximation coefficient function and detail coefficient function, respectively. The function $W_f^\varepsilon(0, t)$ is expressed by

$$\begin{aligned}W_f^\varepsilon(0, t) &= \int_{-\infty}^{\infty} f(\tau) \overline{\phi_1(\tau - t)} d\tau \\ &= F^{-1}(\hat{f}(\omega) \hat{\phi}_1(\omega))\end{aligned}\quad (10)$$

where the overbar denotes complex conjugation and F^{-1} denotes the inverse Fourier transform of a function.

Note that $F^{-1}(\hat{\phi}_1(\omega)) = \phi_1(t)$ and $F^{-1}(\hat{\psi}_n(\omega)) = \psi_n(t)$. The function $W_f^\varepsilon(n, t)$ is expressed by

$$\begin{aligned}W_f^\varepsilon(n, t) &= \int_{-\infty}^{\infty} f(\tau) \overline{\psi_n(\tau - t)} d\tau \\ &= F^{-1}(\hat{f}(\omega) \hat{\psi}_n(\omega))\end{aligned}\quad (11)$$

Resulting decomposed components of the signal can be expressed by

$$f_0(t) = W_f^\varepsilon(0, t) * \phi_1(t) \quad (12)$$

$$f_n(t) = W_f^\varepsilon(n, t) * \psi_n(t) \quad (13)$$

A step-by-step description of the EWT for a signal $f(t)$ is provided as follows

Step 1. Obtain a frequency spectrum of $f(t)$ using Fourier transform.

Step 2. Segment the frequency spectrum in Step 1 using the segmentation technique, such as the local maxima technique and lowest minimum technique.

Step 3. Construct a wavelet filter bank based on the frequency segments in Step 2.

Step 4. Express approximation and detail coefficient functions based on the wavelet filter bank in Step 3.

Step 5. Decompose $f(t)$ and reconstruct it as $\tilde{f}(t)$ in Eq. (9).

The EWT can yield accurate decomposition results when $f(t)$ does not have closely-spaced modes. However, when $f(t)$ has closely-spaced modes, a mode mixing problem can occur due to the transition phase,

and the problem can become more serious when the closely-spaced modes exist in high frequencies as τ_n becomes larger there.

2.2 FDM

Assume that $f(t)$ is zero-mean and its a discrete form is denoted by $f(u)$, where $f(u)$ is a length-limited signal within one period U , which is an even integer; the fundamental frequency of $f(u)$ can be expressed by

$$\varphi_0 = \frac{2\pi}{U} \quad (14)$$

In the FDM, $f(u)$ is approximated by a summation of K orthogonal FIBFs $g_k(u)$ [20]:

$$f(u) = \sum_{k=1}^K g_k(u) \quad (15)$$

Based on Eq. (15), the analytical signal [24] of $f(u)$ can be expressed by

$$\begin{aligned} z(u) &= f(u) + jH(f(u)) \\ &= \sum_{k=1}^K [g_k(u) + jH(g_k(u))] \\ &= \sum_{k=1}^K z_k(u) \end{aligned} \quad (16)$$

where $H(\cdot)$ denotes Hilbert transform of a function, $j = \sqrt{-1}$, $z_k(u) = g_k(u) + jH(g_k(u))$. The term $z_k(u)$ can be considered as the analytical signal corresponding to $g_k(u)$. Note that $z(u)$ can be estimated as Fourier series:

$$z(u) = \sum_{m=1}^{U/2-1} a_m e^{jm\varphi_0 u} \quad (17)$$

where

$$a_m = \frac{2}{U} \sum_{u=0}^{U-1} f(u) e^{-jm\varphi_0 u} \quad (18)$$

and values of a_m can be estimated using Fourier transform.

The analytical signal $z_k(u)$ can be considered as a filtered signal by Hilbert transform filter [25], which is the counterpart of a filter in the wavelet filter bank in the EWT, and $z_k(u)$ can be further expressed by

$$z_k(u) = \sum_{m=M_{k-1}+1}^{M_k} a_m e^{jm\varphi_0 u} \quad (19)$$

where M_k ranges from 1 to $(U/2-1)$ with $M_0 = 0$. Determination of values of M_k is similar to the segmentation in the EWT. In the FDM, two frequency scan techniques have been proposed to determine the values of M_k in

Eq. (19), including the LTH technique and the HTL technique [20]. Flowcharts of the LTH and HTL techniques are shown in Figs. 2 and 3, respectively. In the LTH technique, K values of M_k are searched in a forward manner so that $M_1 < M_2 < \dots < M_k \dots < M_K$, with which

$$\begin{aligned} z_1(u) &= \sum_{m=M_0}^{M_1} a_m e^{jm\phi_0 u} \\ z_2(u) &= \sum_{m=M_1+1}^{M_2} a_m e^{jm\phi_0 u} \\ &\vdots \\ z_K(u) &= \sum_{m=M_{K-1}+1}^{M_K} a_m e^{jm\phi_0 u} \end{aligned} \quad (20)$$

and $M_K = U/2 - 1$ and $M_0 = 0$. The filtered signal $z_k(u)$ can further be expressed by

$$z_k(u) = A_k(u) e^{j\theta_k(u)} \quad (21)$$

where

$$A_k(u) = \left\| \sum_{m=M_{k-1}+1}^{M_k} a_m e^{jm\phi_0 u} \right\|_2 \quad (22)$$

and

$$\theta_k(u) = \arg \left[\sum_{m=M_{k-1}+1}^{M_k} a_m e^{jm\phi_0 u} \right] \quad (23)$$

denote $A_k(u)$ and $\theta_k(u)$ denote instantaneous amplitude and phase of $z_k(u)$, respectively, in which $\|\cdot\|_2$ and $\arg(\cdot)$ calculate the Euclidean norm and argument of a complex quantity. The FIBFs $g_k(u)$ can be obtained by

$$g_k(u) = \text{Re} \left[A_k(u) e^{j\theta_k(u)} \right] \quad (24)$$

where $\text{Re}(\cdot)$ is the real part of a function. In the HTL technique, K values of M_k are searched in a reverse manner so that $M_K < \dots < M_k < M_{k-1} < \dots < M_1$, with which

$$\begin{aligned} z_1(u) &= \sum_{m=M_1}^{M_0-1} a_m e^{jm\phi_0 u} \\ z_2(u) &= \sum_{m=M_2}^{M_1-1} a_m e^{jm\phi_0 u} \\ &\vdots \\ z_K(u) &= \sum_{m=M_K}^{M_{K-1}-1} a_m e^{jm\phi_0 u} \end{aligned} \quad (25)$$

and $M_0 = U/2$, $M_K = 1$.

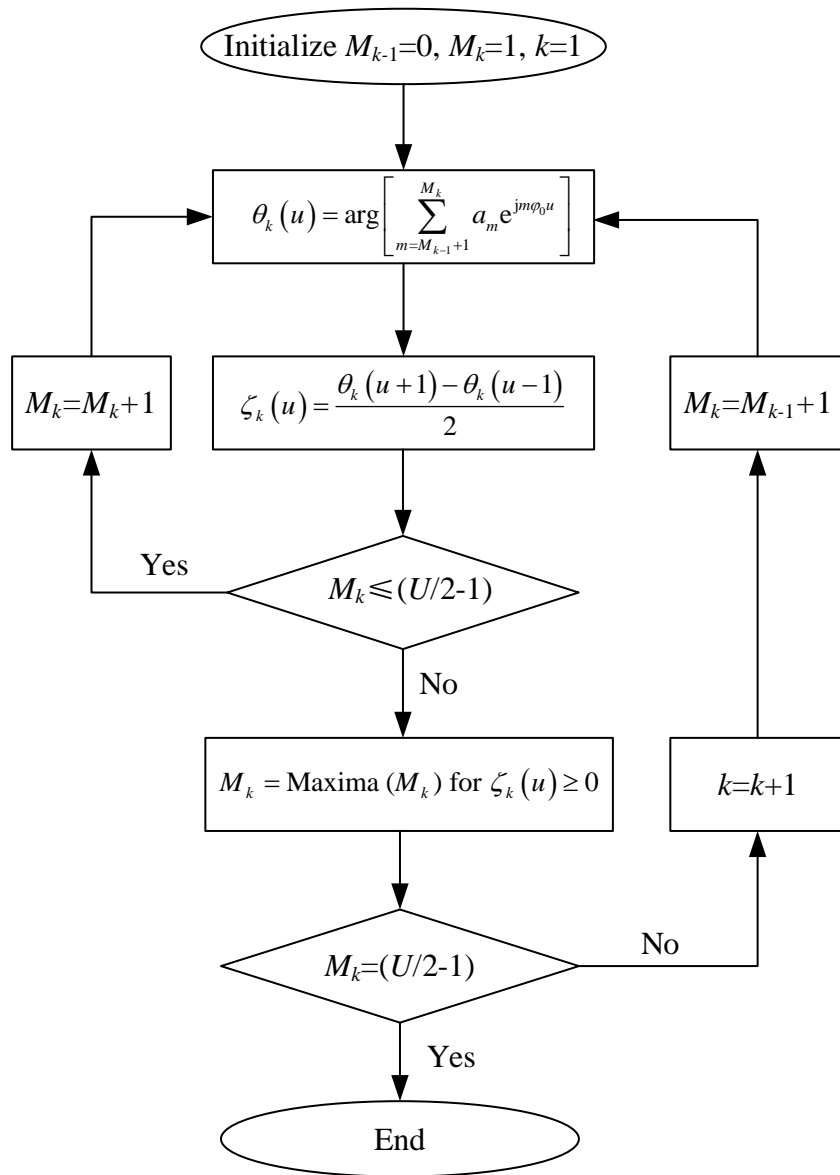


Fig. 2. Flowchart of the LTH technique.

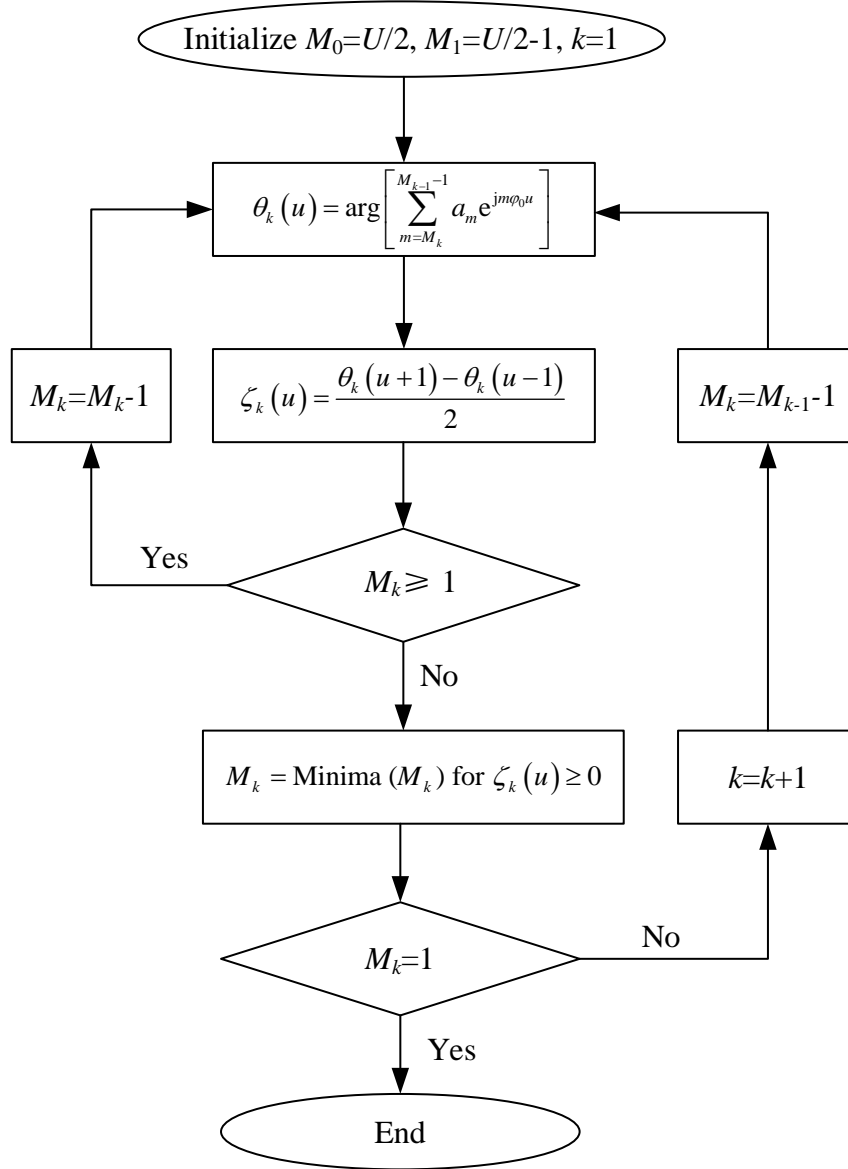


Fig. 3. Flowchart of the HTL technique.

A step-by-step description of the FDM for $f(u)$ is as follows

Step 1. Obtain Fourier spectrum of $f(u)$ using Fourier transform.

Step 2. Express $z(u)$ using the Fourier spectrum of $f(u)$ obtained in Step 1.

Step 3. Obtain $z_k(u)$ using the LTH or HTL technique.

Step 4. Obtain FIBFs $g_k(u)$ from the real part of $z_k(u)$ obtained in Step 3.

An issue of the FDM is that its decomposition results using the LTH technique can be inconsistent with that using the HTL technique, and the issue will be verified in the numerical investigation in Sec. 4.

3. EFD

Similar to the EWT and FDM, the EFD consists of two critical steps: an improved segmentation technique and construction of an ideal filter bank. In the EFD, Fourier spectrum is also defined on a normalized frequency range $[-\pi, \pi]$ and the improved segmentation technique and ideal filter bank for the spectrum in the frequency range $[0, \pi]$ are described below.

3.1 Improved segmentation technique

The improved segmentation technique is proposed based on the lowest minima technique [23] described in Sec. 2.1. In the improved segmentation technique, $[0, \pi]$ is divided into N contiguous frequency segments. Unlike the local maxima and lowest minima techniques, ω_0 and ω_N are not necessarily equal to 0 and π , respectively, and their values are determined in an adaptive sorting process. In the sorting process, Fourier spectrum magnitudes at $\omega = 0$ and $\omega = \pi$ and their local maxima are identified and extracted to a series. All magnitudes in the series are sorted in a descending order. Frequencies corresponding to the first N largest values in the sorted series are denoted by $[\Omega_1, \Omega_2, \dots, \Omega_N]$. In addition, $\Omega_0 = 0$ and $\Omega_{N+1} = \pi$ are defined. Boundaries of each segment are determined by

$$\omega_n = \begin{cases} \arg \min_{\omega} \tilde{X}_n(\omega) & \text{if } 0 \leq n \leq N \text{ and } \Omega_n \neq \Omega_{n+1} \\ \Omega_n & \text{if } 0 \leq n \leq N \text{ and } \Omega_n = \Omega_{n+1} \end{cases} \quad (26)$$

where $\tilde{X}_n(\omega)$ denotes Fourier spectrum magnitudes between Ω_n and Ω_{n+1} , which concludes the improved segmentation technique.

3.2 Construction of filter bank

Both the EWT and FDM consist of a step of constructing filter bank. In the EWT, a wavelet filter bank is formed by the empirical scaling function and wavelet functions. In the FDM, Hilbert transform filter bank is constructed based on Fourier spectrum of the analytical signal associated with a signal to be decomposed. In the EFD, an ideal filter bank is constructed based on frequency segments obtained by the improved segmentation technique. In each frequency segment, the ideal filter is a band-pass filter with ω_{n-1} and ω_n serving as its cut-off frequencies. Hence, the ideal filter can retain the major Fourier spectrum component in the segment and all other Fourier spectrum components beyond the segment are excluded.

Fourier transform of a signal to be decomposed $f(t)$ is determined as

$$\hat{f}(\omega) = \int_{-\infty}^{\infty} f(t) e^{-j\omega t} dt \quad (27)$$

From Eq. (27), an ideal filter bank can be constructed by $\hat{\mu}_n(\omega)$:

$$\hat{\mu}_n(\omega) = \begin{cases} 1, & \omega_{n-1} \leq |\omega| \leq \omega_n \\ 0, & \text{otherwise} \end{cases} \quad (28)$$

where $1 \leq n \leq N$ and values of ω_n are determined by Eq. (27). Graphical illustrations of the ideal filter bank is shown in Fig. 4.

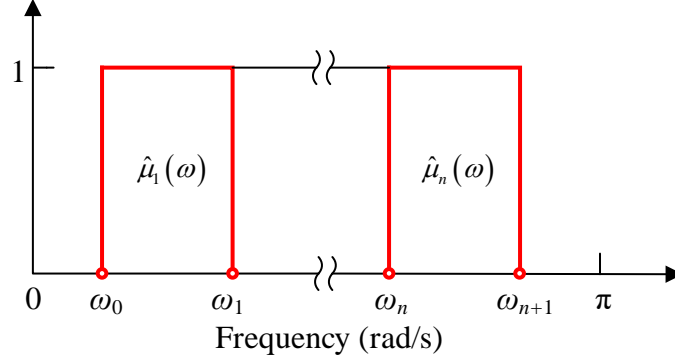


Fig. 4. Graphical illustration of an ideal filter bank of the EFD.

Filtered signals that correspond to $\hat{\mu}_n(\omega)$ are calculated by

$$\hat{f}_n(\omega) = \hat{\mu}_n(\omega) \hat{f}(\omega) = \begin{cases} \hat{f}(\omega), & \omega_{n-1} \leq |\omega| \leq \omega_n \\ 0, & \text{otherwise} \end{cases} \quad (29)$$

Decomposed components in the time domain can be obtained using the inverse Fourier transform:

$$\begin{aligned} f_n(t) &= F^{-1}[\hat{f}_n(\omega)] = \int_{-\infty}^{\infty} \hat{f}_n(\omega) e^{j\omega t} d\omega \\ &= \int_{-\omega_n}^{-\omega_{n-1}} \hat{f}(\omega) e^{j\omega t} d\omega + \int_{\omega_{n-1}}^{\omega_n} \hat{f}(\omega) e^{j\omega t} d\omega \end{aligned} \quad (30)$$

The reconstructed signal is calculated as a summation of all decomposed components:

$$\tilde{f}(t) = \sum_{n=1}^N f_n(t) \quad (31)$$

A flowchart of the EFD is shown in Fig. 5 and a step-by-step description of the EFD is provided as follows.

Step 1. Obtain the Fourier spectrum of signal to be decomposed $f(t)$ using Fourier transform.

Step 2. Determine boundaries of segment ω_n using the improved segmentation technique based on the Fourier spectrum obtained in Step 1.

Step 3. Construct an ideal filter bank $\hat{\mu}_n(\omega)$ based on ω_n obtained in Step 2.

Step 4. Acquire filtered signals $\hat{f}_n(\omega)$ in the frequency domain using $\hat{\mu}_n(\omega)$ obtained in Step 3.

Step 5. Obtain decomposed components $f_n(t)$ in the time-domain using inverse Fourier transforms of $\hat{f}_n(\omega)$ obtained in Step 4

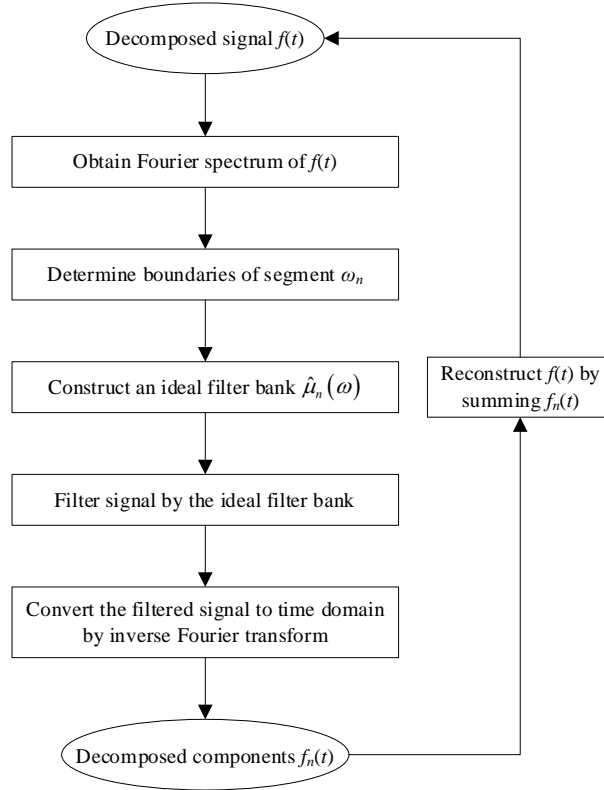


Fig. 5. Flowchart of the EFD.

4. Numerical investigation

In this section, the effectiveness of the lowest minima and improved segmentation techniques are compared based on two typical signals that have multiple modes, denoted by $f_{Sig1}(t)$ and $f_{Sig2}(t)$. Decomposition accuracy of the proposed EFD method is compared with those of the EWT [16], FDM [20], VMD [13] and EMD [7] methods for two typical non-stationary time-domain signals $f_{Sig3}(t)$ and $f_{Sig4}(t)$, and two stationary time-domain signals $f_{Sig5}(t)$ and $f_{Sig6}(t)$, which are used to study the closely-spaced modes. For the EFD, EWT and VMD, the numbers of decomposed modes are listed in Table 1.

Table 1 Number of modes to be decomposed.

Signal	Decomposition method		
	EFD	EWT	VMD
$f_{Sig1}(t)$	3	3	-
$f_{Sig2}(t)$	3	4	-

$f_{\text{Sig3}}(t)$	2	2	2
$f_{\text{Sig4}}(t)$	3	3	3
$f_{\text{Sig5}}(t)$	3	4	3
$f_{\text{Sig6}}(t)$	2	3	2

4.1 Comparison of segmentation techniques

The signals $f_{\text{Sig1}}(t)$ and $f_{\text{Sig2}}(t)$ are expressed by

$$f_{\text{Sig1}}(t) = 6t + \cos(24\pi t) + \cos(50\pi t) + \delta(t) \quad (32)$$

$$f_{\text{Sig2}}(t) = \cos(20\pi t) + \cos(24\pi t) + \cos(50\pi t) + \delta(t) \quad (33)$$

where $\delta(t)$ is a random white-noise such that $f_{\text{Sig1}}(t)$ and $f_{\text{Sig2}}(t)$ have signal-to-noise-ratios of 10 dB. Segmentation results of $f_{\text{Sig1}}(t)$ by the lowest minima and improved segmentation techniques are shown in Fig. 6: the first two segments S_1 and S_2 by the two techniques are the same, but S_3 in the improved segmentation technique has a smaller frequency range than that by the lowest minima technique. Therefore, the improved segmentation technique can alleviate the effect of noise on the decomposed component associated with the last segment. Segmentation results of $f_{\text{Sig2}}(t)$ by the lowest minima and improved segmentation techniques are shown in Fig. 7. S_1 by the lowest minima technique, shown in Fig. 7(a), can be considered trivial as it does not contain a meaningful Fourier spectrum component and its associated decomposed component consists of noise. However, the trivial segment is not contained in segmentation results by the improved segmentation technique, shown in Fig. 7(b), and its first resulting component contains a meaningful Fourier spectrum component. Segmentation results of the last segments by the lowest minima and improved segmentation techniques are similar to those of $f_{\text{Sig1}}(t)$: the decomposed component associated with the improved segmentation technique has a lower level of noise.

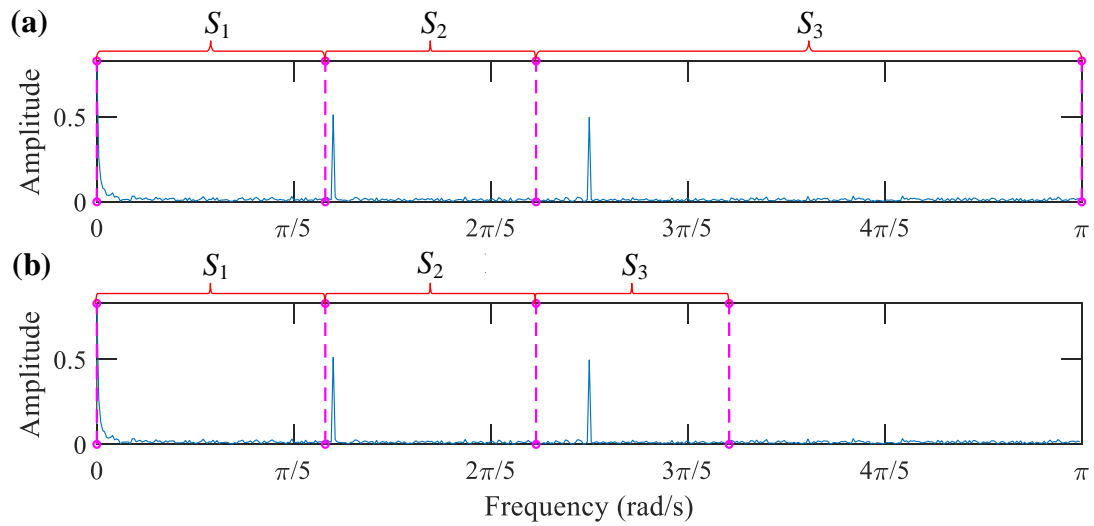


Fig. 6. Segmentation results of $f_{\text{Sig1}}(t)$: (a) the lowest minima technique, (b) the improved segmentation technique.

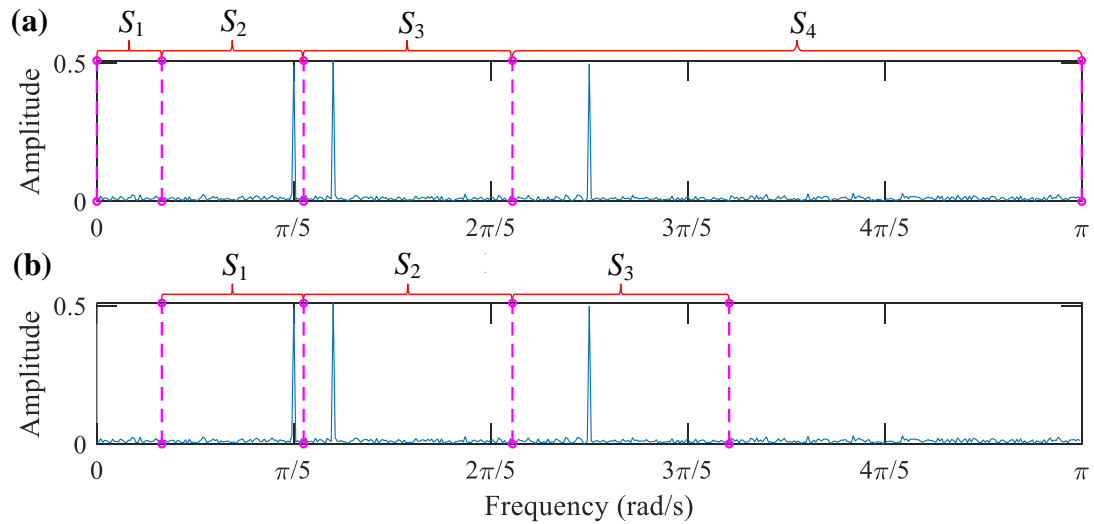


Fig. 7. Segmentation results of $f_{\text{Sig2}}(t)$: (a) the lowest minima technique, (b) the improved segmentation technique.

4.2 Non-stationary multimode signals

The first non-stationary multimode signal denoted by $f_{\text{Sig3}}(t)$ is expressed by

$$\begin{cases} f_{\text{Sig3C1}}(t) = \frac{1}{1.2 + \cos(2\pi t)} \\ f_{\text{Sig3C2}}(t) = \frac{\cos(32\pi t + 0.2 \cos(64\pi t))}{1.5 + \sin(2\pi t)} \\ f_{\text{Sig3}}(t) = f_{\text{Sig3C1}}(t) + f_{\text{Sig3C2}}(t) \end{cases} \quad (34)$$

The signal $f_{\text{Sig3}}(t)$ consists of two modes that are shown in Figs. 8(a) and (b) [26], and the expression of $f_{\text{Sig3}}(t)$

is similar to that of a solution to Duffing equation [7]. The signal $f_{\text{Sig}3}(t)$ is sampled at a frequency of 1000 Hz for one second and shown in Fig. 8(c).

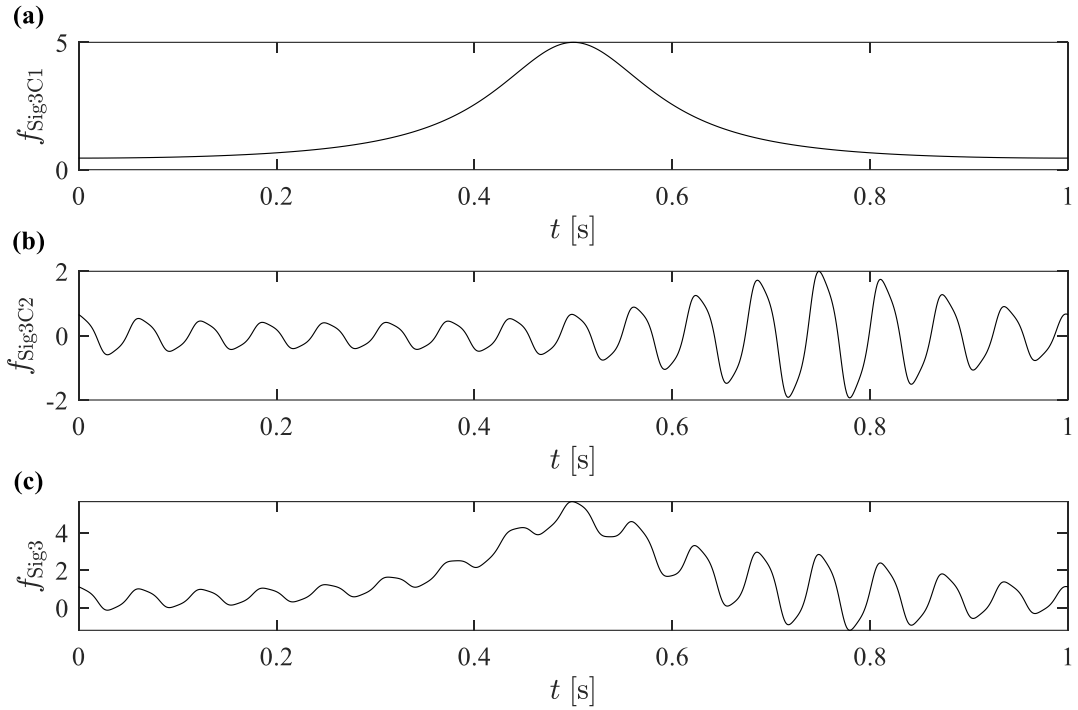


Fig. 8. (a) Modes $f_{\text{Sig}3\text{C}1}$, (b) $f_{\text{Sig}3\text{C}2}$ and (c) the non-stationary signal $f_{\text{Sig}3}$ that consists of the two modes in (a) and (b) as expressed in Eq. (34).

Decomposition results of $f_{\text{Sig}3}(t)$ by the EFD, EWT, FDM-LTH, FDM-HTL, VMD, and EMD are shown in Fig. 9. Root-mean-square errors (RMSEs) between the decomposition results and analytical ones are calculated by

$$\text{RMSE} = \sqrt{\frac{1}{R} \sum_{r=1}^R |y_r - \tilde{y}_r|^2} \quad (35)$$

where y_r is the analytical component at the r -th discrete instant, and \tilde{y}_r is the corresponding component at the r -th discrete instant obtained by a decomposition method. RMSEs associated with the aforementioned decomposition methods are calculated and listed in Table 2. For $f_{\text{Sig}3\text{C}1}$, it can be seen that the RMSE associated with the EMD is the smallest and that associated with the EFD is the second smallest. While the RMSEs associated with the EWT, VMD and FDM-LTH are relatively small, that associated with the FDM-HTL is large. For $f_{\text{Sig}3\text{C}2}$, results similar to $f_{\text{Sig}3\text{C}1}$ can be observed: RMSEs associated with the EMD and EFD are the smallest, and the RMSEs of the EWT, VMD and FDM-LTH are relatively small. In addition, the RMSE associated with the FDM-HTL is also large. It is indicated that the EFD can accurately decompose the non-

stationary multimode signal. The inconsistency of decomposition results by the FDM-LTH and FDM-HTL is verified.

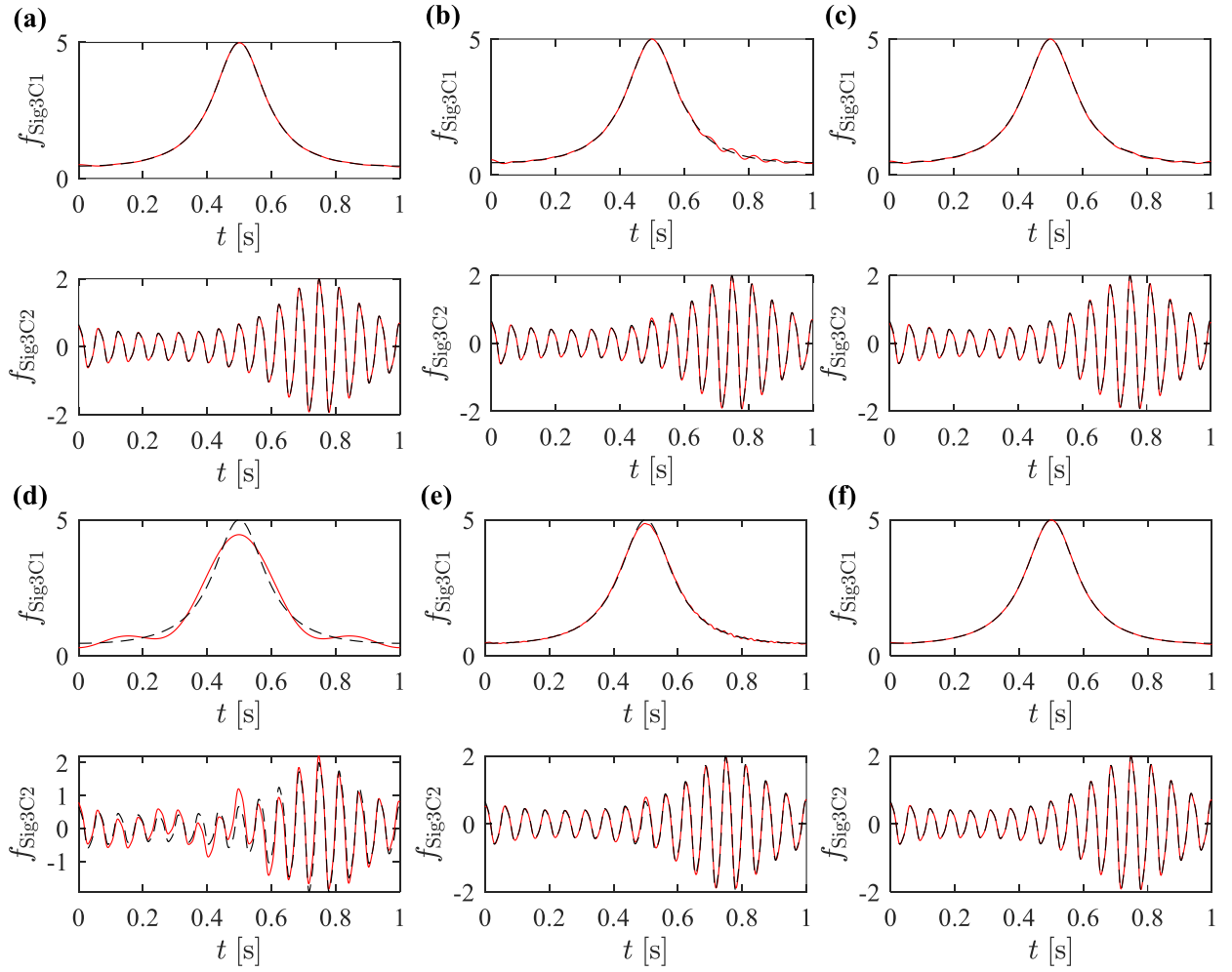


Fig. 9. Comparisons between the analytical components of $f_{\text{Sig}3}(t)$ (dashed lines) in Eq. (34) and decomposition results of $f_{\text{Sig}3}$ (solid line) by the (a) EFD, (b) EWT, (c) FDM-LTH, (d) FDM-HTL, (e) VMD, and (f) EMD.

Table 2 Results of the RMSEs for $f_{\text{Sig}3}(t)$.

Component	Decomposition method					
	EFD	EWT	FDM-LTH	FDM-HTL	VMD	EMD
$f_{\text{Sig}3\text{C}1}$	1.12×10^{-2}	4.19×10^{-2}	2.43×10^{-2}	2.11×10^{-1}	3.74×10^{-2}	9.54×10^{-3}
$f_{\text{Sig}3\text{C}2}$	9.85×10^{-3}	2.12×10^{-2}	7.89×10^{-2}	2.24×10^{-1}	5.41×10^{-2}	9.54×10^{-3}

The second non-stationary multimode signal denoted by $f_{\text{Sig}4}(t)$ is expressed by [26]

$$\begin{cases} f_{\text{Sig4C1}}(t) = 6t \\ f_{\text{Sig4C2}}(t) = \cos(8\pi t) \\ f_{\text{Sig4C3}}(t) = 0.5 \cos(40\pi t) \\ f_{\text{Sig4}}(t) = f_{\text{Sig4C1}}(t) + f_{\text{Sig4C2}}(t) + f_{\text{Sig4C3}}(t) \end{cases} \quad (36)$$

The signal $f_{\text{Sig4}}(t)$ consists of three modes: one mode with a monotonically increasing amplitude as shown in Fig. 10(a) and two modes with sinusoidal amplitudes as shown in Figs. 10(b) and (c). The signal $f_{\text{Sig4}}(t)$ is sampled at a frequency of 1000 Hz for one second and shown in Fig. 10(d).

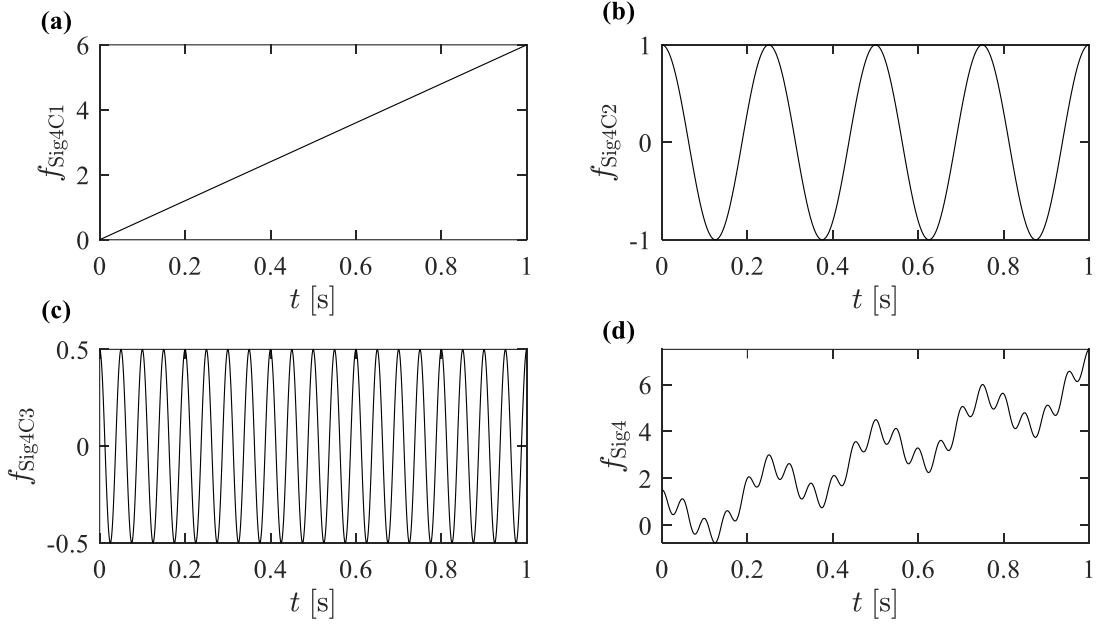


Fig. 10. (a) Modes f_{Sig4C1} , (b) f_{Sig4C2} , (c) f_{Sig4C3} and (d) the non-stationary signal f_{Sig4} that consists of the three modes in (a), (b) and (c) as expressed in Eq. (36).

The EFD, EWT, FDM-LTH, FDM-HTL, VMD and EMD are employed to decompose the sampled $f_{\text{Sig4}}(t)$. Their results are compared with the analytical ones as shown in Fig. 11 and corresponding RMSEs in Eq. (35) are calculated and listed in Table 3. For f_{Sig4C1} , the RMSE associated with the EFD is the smallest, and those associated with the EWT, VMD and EMD are relatively small. RMSES associated the FDM-LTH and FDM-HTL are large. For f_{Sig4C2} , RMSE associated the EMD is the smallest and those associated with the EFD and VMD are slightly larger than that associated with the EMD. The RMSEs associated with the EWT, FDM-LTH and FDM-HTL are large and that associated with the FDM is the largest. For f_{Sig4C3} , the RMSE associated with the EFD is the smallest while those associated with the VMD and EMD are slightly larger than that associated with the EFD. Similar to the observations for f_{Sig4C2} , the RMSEs associated with the EWT, FDM-TLH and FDM-HTL are larger than others. It is indicated again that the EFD can accurately decompose a nonstationary multimode signal. In addition, it is shown that both the FDM-LTH and FDM-HTL can yield inaccurate

decomposition results.

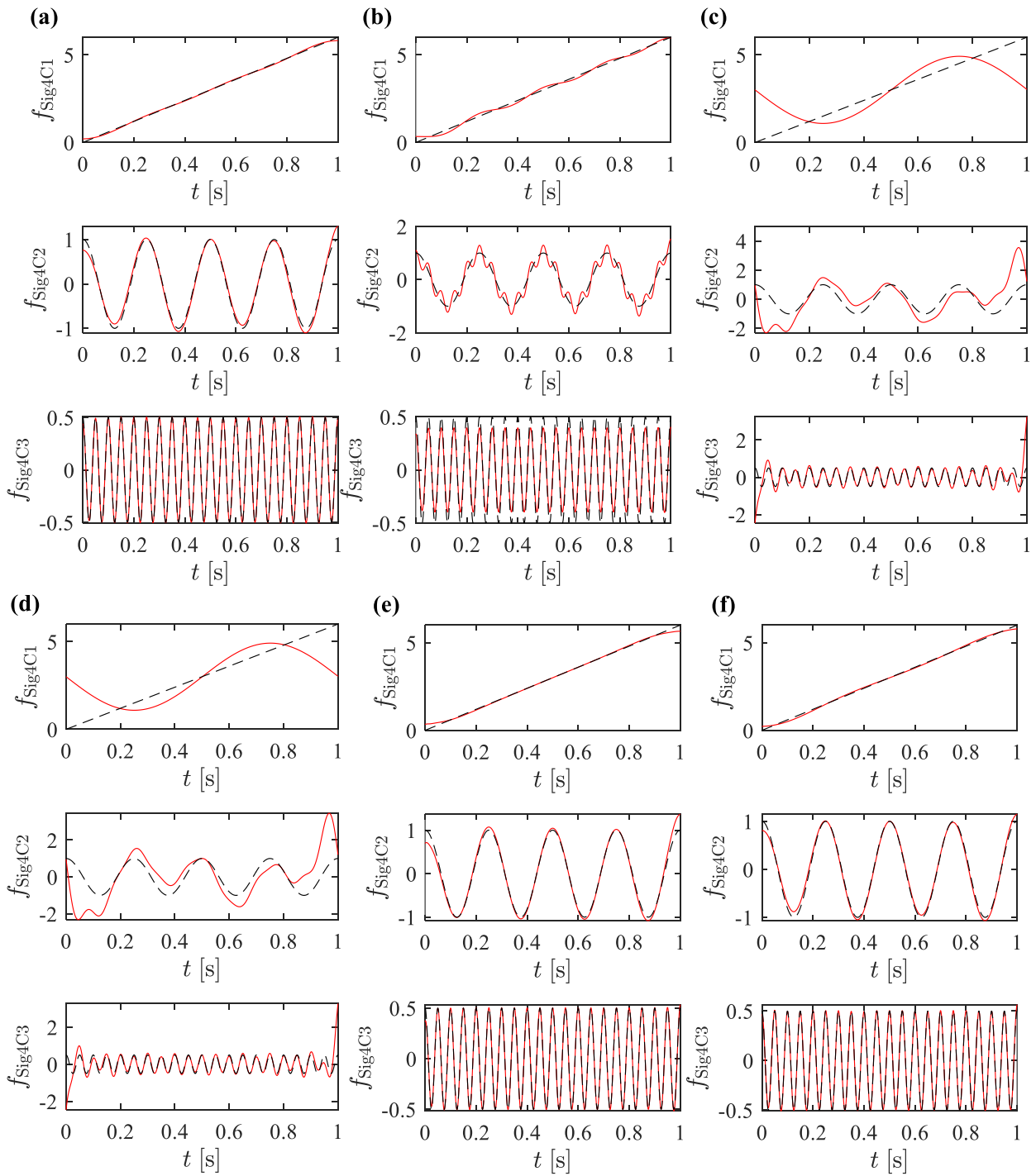


Fig. 11. Comparisons between the analytical components of f_{Sig4} (dashed lines) in Eq. (36) and decomposition results of f_{Sig4} (solid line) by the (a) EFD, (b) EWT, (c) FDM-LTH, (d) FDM-HTL, (e) VMD, and (f) EMD.

Table 3 Results of the RMSEs in $f_{\text{Sig4}}(t)$.

Component	Method					
	EFD	EWT	FDM-LTH	FDM-HTL	VMD	EMD
f_{Sig4C1}	4.67×10^{-2}	1.07×10^{-1}	1.08×10^0	1.08×10^0	8.40×10^{-2}	6.46×10^{-2}
f_{Sig4C2}	8.33×10^0	2.23×10^{-1}	1.02×10^0	1.02×10^0	9.14×10^{-2}	6.38×10^{-2}
f_{Sig4C3}	7.01×10^{-1}	7.43×10^{-2}	3.81×10^{-1}	3.98×10^{-1}	9.93×10^{-3}	8.10×10^{-3}

4.3 Closely-spaced modes

A stationary multimode signal denoted by $f_{\text{Sig5}}(t)$ is expressed

$$\begin{cases} f_{\text{Sig5C1}}(t) = \cos(2\pi\lambda_a t) \\ f_{\text{Sig5C2}}(t) = \cos(2\pi\lambda_b t) \\ f_{\text{Sig5C3}}(t) = \cos(2\pi\lambda_c t) \\ f_{\text{Sig5}}(t) = f_{\text{Sig5C1}}(t) + f_{\text{Sig5C2}}(t) + f_{\text{Sig5C3}}(t) \end{cases} \quad (37)$$

where $\lambda_a=1.1$ Hz, $\lambda_b=1.3$ Hz and $\lambda_c=3.1$ Hz, and it consists of a pair of closely-spaced modes shown in Figs. 12(a) and (b) and a mode with a frequency greatly larger than those of the closely-spaced modes shown in Fig. 12(c). The signal $f_{\text{Sig5}}(t)$ is sampled at a frequency of 50 Hz for 20 seconds and shown in Fig. 12(d).

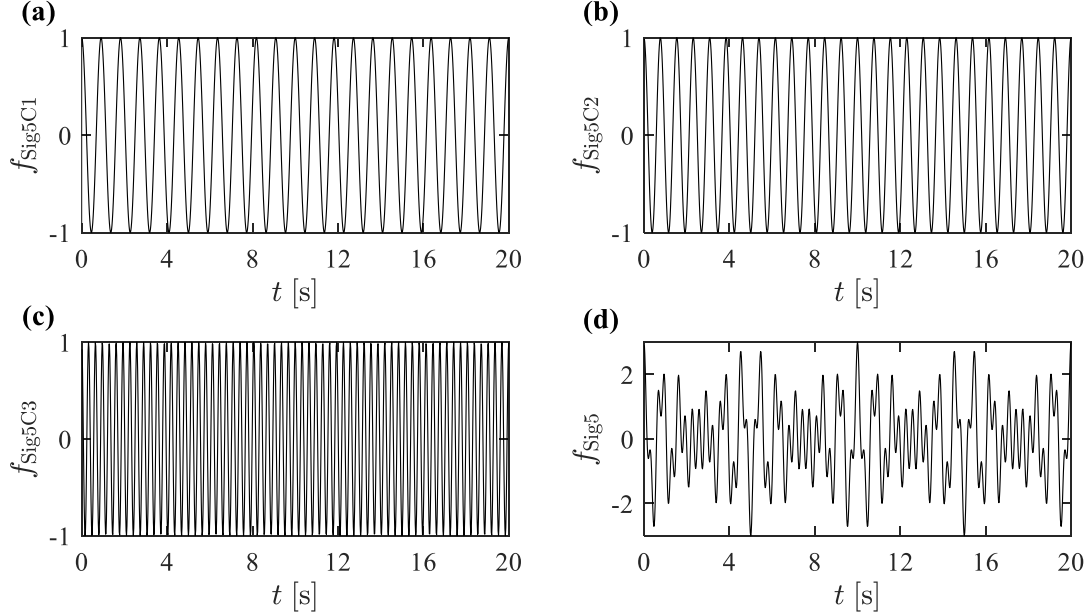


Fig. 12. (a) Modes f_{Sig5C1} , (b) f_{Sig5C2} , (c) f_{Sig5C3} , and (d) f_{Sig5} that consists of the three modes in (a), (b) and (c) which are expressed in Eq. (37).

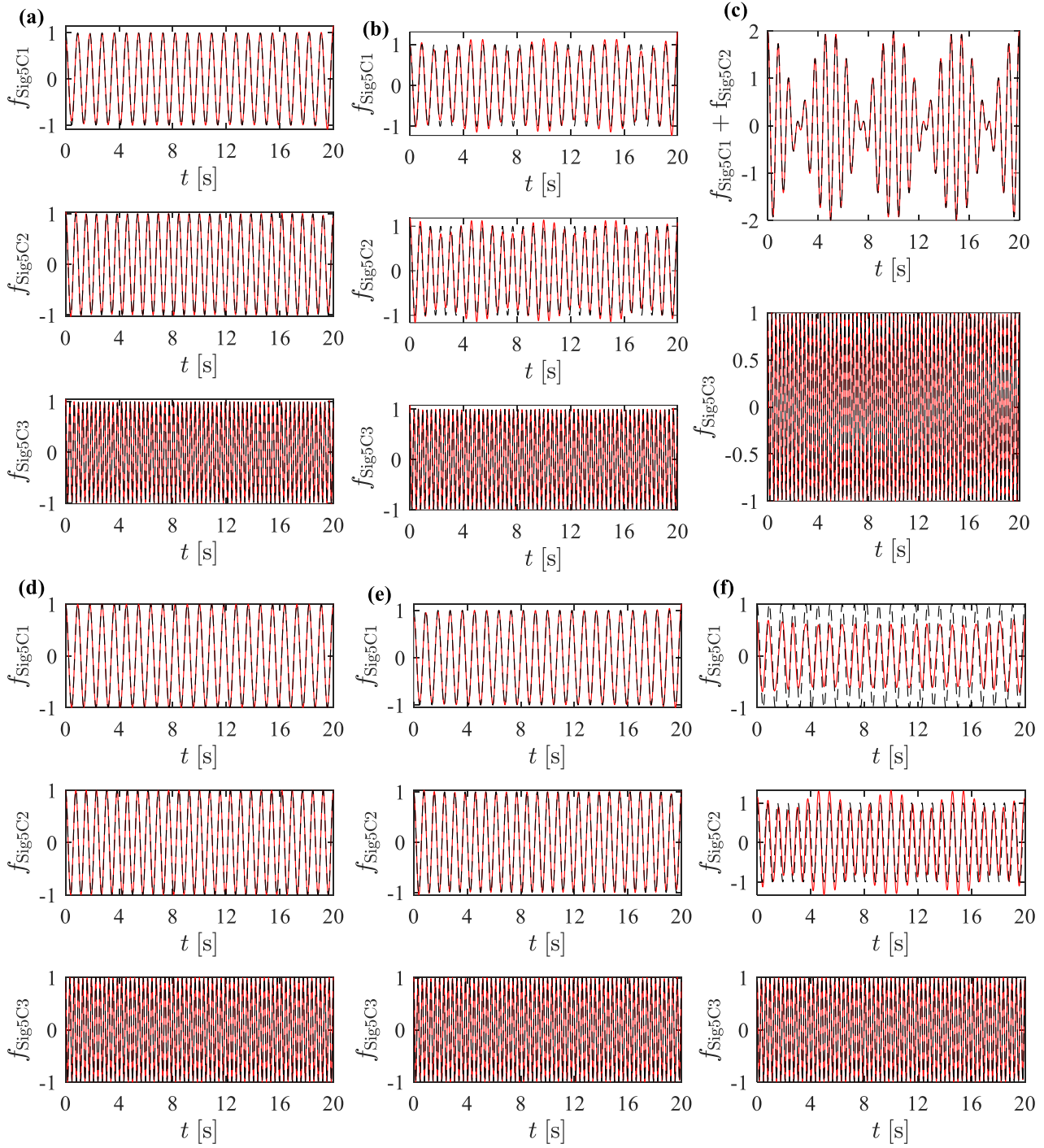


Fig. 13. Comparisons between the analytical components of $f_{\text{Sig}5}$ (dashed lines) in Eq. (37) and decomposition results of $f_{\text{Sig}5}$ (solid line) by the (a) EFD, (b) EWT, (c) FDM-LTH, (d) FDM-HTL, (e) VMD, and (f) EMD.

The EFD, EWT, FDM-LTH, FDM-HTL, VMD, and EMD are used to decompose the sampled $f_{\text{Sig}5}(t)$. Their results are shown in Fig. 13 and corresponding RMSEs in Eq. (35) are calculated and listed in Table 4.

Note that in the decomposition results by the FDM-LTH, only two components are obtained as f_{Sig5C1} and f_{Sig5C2} exist in the first component and RMSEs corresponding to f_{Sig5C1} and f_{Sig5C2} cannot be differentiated. For f_{Sig5C1} , the RMSE associated with the FDM-HTL is the smallest and those associated with the VMD and EFD are relatively small, and those associated with the EWT, FDM-LTH and EMD are large. For f_{Sig5C2} , similar observations can be obtained: the RMSE associated with the FDM-HTL is the smallest, those associated with the VMD and EFD are relatively small, and those associated with EWT, FDM-LTH and EMD are large. For f_{Sig5C3} , the RMSEs associated with the FDM-LTH and FDM-HTL are the smallest and those associated with other methods are relatively small. It is indicated that the EFD can yield decomposition results for signals with closely-spaced modes with higher accuracy than the EWT and EMD. In addition, the inconsistency between decomposition results by the FDM-LTH and FDM-HTL is verified again.

Table 4 Results of RMSEs for $f_{\text{Sig5}}(t)$.

Component	Decomposition method					
	EFD	EWT	FDM-LTH	FDM-HTL	VMD	EMD
f_{Sig5C1}	2.20×10^{-2}	1.11×10^{-1}	7.07×10^{-1}	0.00	1.90×10^{-2}	7.02×10^{-1}
f_{Sig5C2}	1.60×10^{-2}	1.10×10^{-1}	7.07×10^{-1}	0.00	1.50×10^{-2}	6.94×10^{-1}
f_{Sig5C3}	1.20×10^{-2}	1.20×10^{-2}	0.00	0.00	1.41×10^{-2}	4.58×10^{-2}

Next, a stationary multimode signal with two modes [27] denoted by $f_{\text{Sig6}}(t)$ is constructed to further compare performances of the different decomposition methods, which is expressed by

$$\begin{cases} f_{\text{Sig6C1}}(t) = \cos(2\pi t) \\ f_{\text{Sig6C2}}(t) = a \cos(2\pi \lambda_r t) \\ f_{\text{Sig6}}(t) = f_{\text{Sig6C1}}(t) + f_{\text{Sig6C2}}(t) \end{cases} \quad (38)$$

where a and λ_r denote a ratio between the amplitudes of $f_{\text{Sig6C2}}(t)$ and $f_{\text{Sig6C1}}(t)$ and that between the frequencies of $f_{\text{Sig6C2}}(t)$ and $f_{\text{Sig6C1}}(t)$, respectively; $0.01 \leq a \leq 100$ and $0.01 \leq \lambda_r \leq 1$. When λ_r approaches to 1, $f_{\text{Sig6C2}}(t)$ and $f_{\text{Sig6C1}}(t)$ become closely-spaced modes. The signal $f_{\text{Sig6}}(t)$ is sampled at a frequency of 10 Hz for 300 seconds. The EFD, EWT, FDM-LTH, FDM-HLT, VMD and EMD are deployed to decompose $f_{\text{Sig6}}(t)$. A two-dimensional binary quantity $Q(a, \lambda_r)$ is used to measure the decomposition performance [27] of the different methods for $f_{\text{Sig6}}(t)$ with different values of a and λ_r , which is expressed by

$$Q(a, \lambda_r) = \begin{cases} 0, & \text{if } \frac{\|C1 - f_{\text{Sig6C1}}\|_2}{\|f_{\text{Sig6C2}}\|_2} \leq \varepsilon \\ 1, & \text{if } \frac{\|C1 - f_{\text{Sig6C1}}\|_2}{\|f_{\text{Sig6C2}}\|_2} > \varepsilon \end{cases} \quad (39)$$

where C1 is the decomposed component by a decomposition method corresponding to $f_{\text{Sig6C1}}(t)$ and ε is the threshold of Q . A zero value and a unit value of Q indicate an acceptable and unacceptable decomposition result, respectively, and the value of ε is chosen to be 0.5 in this study, which was also the cases in Refs. [4,12,27]. Resulting $Q(a, \lambda_r)$ corresponding to the six methods are shown in Fig. 14, where the colors of blue and yellow correspond to Q values of 0 and 1, respectively. It can be seen that the yellow area corresponding to the EFD is the smallest among the six Q results. Even as λ_r approaches to 1, $f_{\text{Sig6}}(t)$ can still be well decomposed. However, the decomposition by the EFD is affected when a approaches to 0.01. Further, the yellow area corresponding to the EWT is the second smallest but its decomposition performance is affected when a approaches to 0.01 and λ_r is larger than 0.8. The yellow area corresponding to the VMD is the third smallest. Similar to Q corresponding to the EFD, as λ_r approaches to 1, $f_{\text{Sig6}}(t)$ can still be well decomposed. However, the decomposition performance associated with the VMD is affected when a is close to 0.01 and 100. The yellow area corresponding to the EMD is the fourth smallest. The EMD cannot decompose $f_{\text{Sig6}}(t)$, when λ_r is larger than 0.65 for all a . In addition, worse decomposition results are obtained when a approaches to 100. For the FDM-LTH and FDM-HTL, their decomposition performances are almost the same but the worst among the six methods. Their decomposition results are greatly affected by the value of a . They can hardly decompose $f_{\text{Sig6}}(t)$, when a is smaller than 1 for $\lambda_r \geq 0.01$. Based on the observations, it is indicated that the EFD can well decompose $f_{\text{Sig6}}(t)$ and its decomposition results are best even when $f_{\text{Sig6}}(t)$ becomes a signal with closely-spaced modes and both the FDM-LTH and FDM-HTL can yield inaccurate decomposition results for $f_{\text{Sig6}}(t)$.

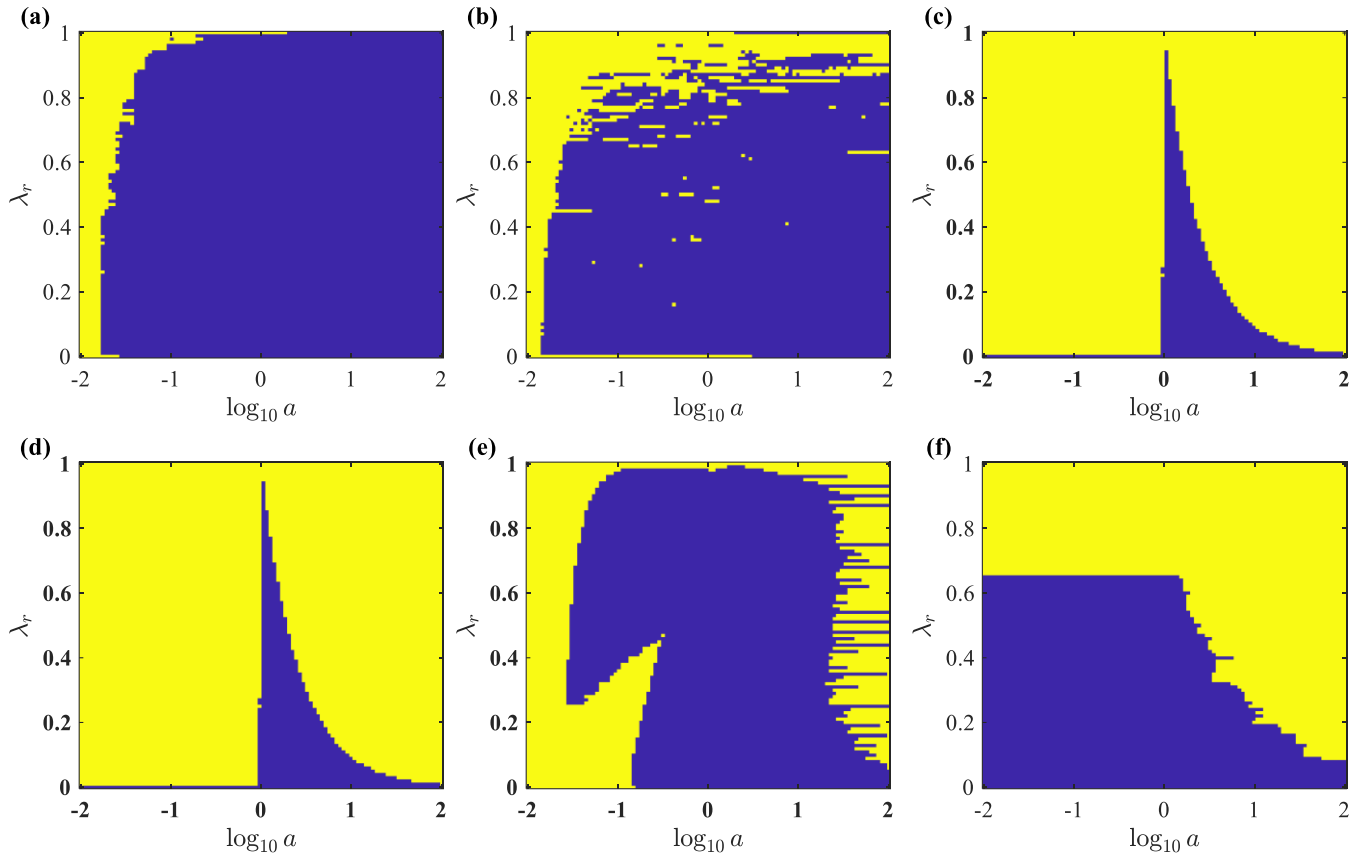


Fig. 14. Decomposition performance with respect to (a, λ_r) by the (a) EFD, (b) EWT, (c) FDM-LTH, (d) FDM-HTL, (e) VMD and (f) EMD

4.4 Time-frequency representation

Time-frequency representations (TFRs) of components decomposed by the six methods are compared to further study their performances. TFR of decomposed components by the EFD, EWT, VMD and EMD are calculated using Hilbert transform and those by the FDM-HTL and FDM-LTH are directly obtained as $A(u)$ and $\zeta(u)$. A benchmark TFR is obtained as the sum of Hilbert transforms of $f_{\text{sig3C1}}(t)$ and $f_{\text{sig3C2}}(t)$. TFRs corresponding to six decomposition methods and the benchmark one are shown in Fig. 15 and RMSEs corresponding to TFR are calculated and listed in Table 5. From Fig. 15, it can be found that the TFRs associated with the EFD and FDM-LTH compare well with the benchmark one, while the comparisons between the TFRs associated with the EWT and EMD and the benchmark one are acceptable. However, large differences can be observed between the TFRs associated with the VMD and FDM-HTL and the benchmark one.

In addition, RMSEs of between magnitudes in the TFRs by the six method and those in the benchmark TFR at all frequencies and times are calculated and listed in Table 5. It can be seen that the RMSEs associated with the TFRs by the EFD and EWT are the smallest. Those associated with the TFR by the EMD are relatively

small, while those associated with the TFRs by the FDM-LTH, FDM-HTL and VMD are large. The TFRs shown in Fig. 15 and the RMSEs in Table 5 show that the EFD can yield good estimation for TFR, and the inconsistency between TFR results by the FDM-LTH and FDM-HTL is verified.

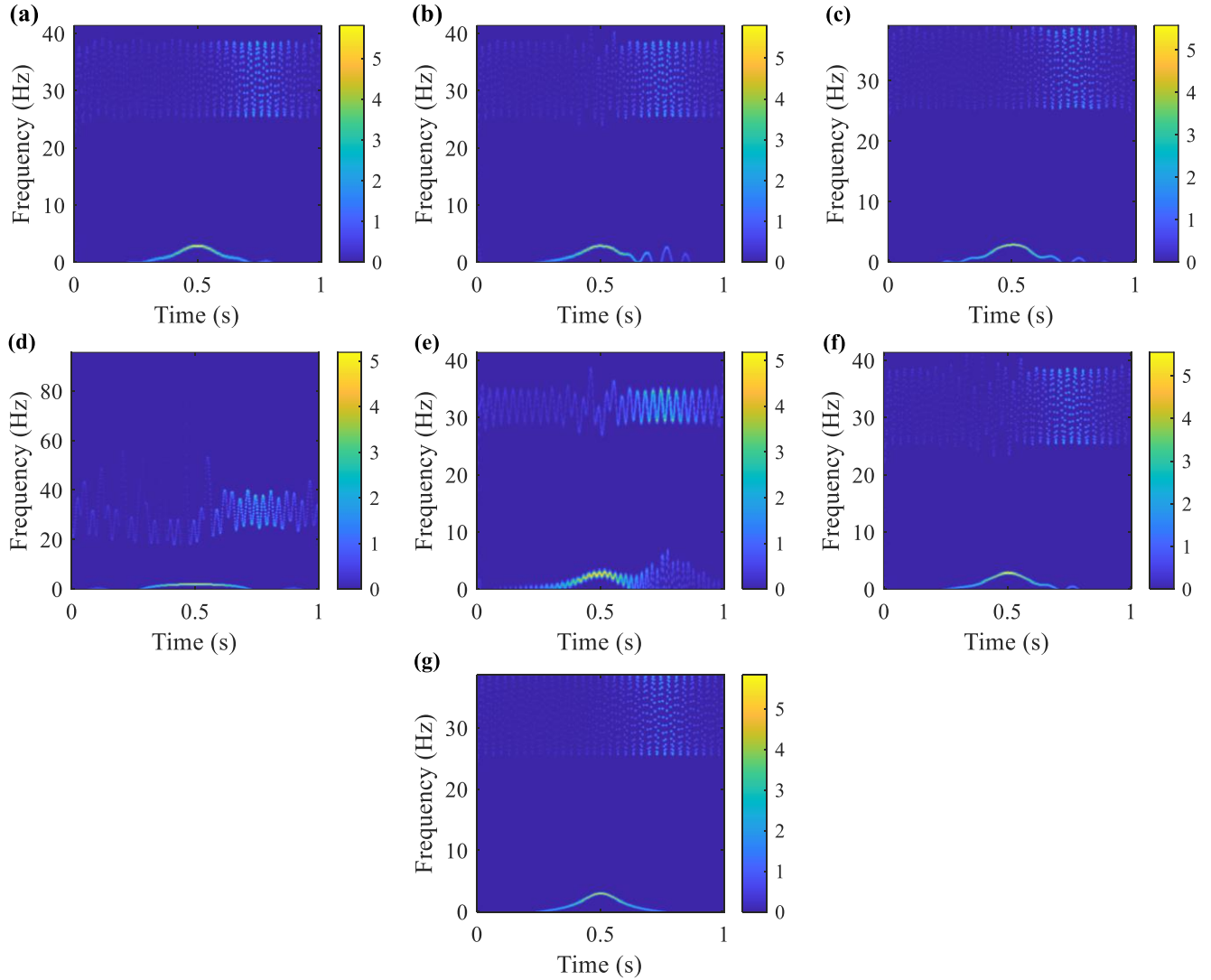


Fig. 15. TFR results of $f_{\text{Sig}3}(t)$ by: (a) EFD, (b) EWT, (c) FDM-LTH, (d) FDM-HTL, (e) VMD, (f) EMD, and (g) benchmark.

Table 5 Calculated RMSEs of TFR associated with $f_{\text{Sig}3}(t)$.

EFD	EWT	FDM-LTH	FDM-HTL	VMD	EMD
1.24×10^{-1}	1.24×10^{-1}	1.35×10^{-1}	1.38×10^{-1}	1.36×10^{-1}	1.29×10^{-1}

4.5 Computational cost

To explore the computational cost of the EFD, computation time by the EFD, EWT, FDM, VMD and EMD for $f_{\text{Sig}3}(t)$, $f_{\text{Sig}4}(t)$ and $f_{\text{Sig}5}(t)$ are compared as listed in Table 6. All computations are conducted on a PC with an Intel Xeon W-2123 CPU, 16.0 GB of RAM, 64-bit Windows 10, and software of MATLAB R2020a.

It can be seen that the EFD requires the shortest computation time among the six methods. The computation times associated with the EFD and EWT are comparable and while those of the FDM-HTL and FDM-LTW are large. The computational times of the VMD and EMD depended on their parameters. Though they can greatly vary, they are longer than that of the EFD.

Table 6 Computation time for $f_{\text{Sig3}}(t)$, $f_{\text{Sig4}}(t)$ and $f_{\text{Sig5}}(t)$ by the EFD, EWT, FDM-LTH, FDM-HTL, VMD and EMD.

Signal	Computation Time (s)					
	EFD	EWT	FDM-LTH	FDM-HTL	VMD	EMD
$f_{\text{Sig3}}(t)$	1.7×10^{-2}	6.3×10^{-2}	1.75×10^{-1}	1.09×10^{-1}	1.75×10^{-1}	8.2×10^{-2}
$f_{\text{Sig4}}(t)$	1.5×10^{-2}	6.6×10^{-2}	2.59×10^{-1}	1.04×10^{-1}	1.963×10^{-0}	9.6×10^{-2}
$f_{\text{Sig5}}(t)$	1.7×10^{-2}	7.0×10^{-2}	1.59×10^{-1}	1.16×10^{-1}	1.412×10^{-0}	1.506×10^{-0}

5. Concluding remarks

In this paper, a novel EFD method is proposed to decompose time-domain signals. The EFD can be consists of two critical steps: the improved segmentation technique and construction of a filter bank. In the improved segmentation technique, only meaningful Fourier spectrum components are included and the last segment that can consist of noise is shortened, which can decrease the size of a segment for decomposition and alleviate the adverse effect of noise. In a constructed filter bank, transition phases of filter functions are eliminated, which can improve the decomposition performance in the closely-spaced modes. Two numerical investigations are conducted on the non-stationary signals, and the EFD can yield decomposition results with high accuracy and consistency. Two numerical investigations are conducted on two stationary signals to study the decomposition performance of the EFD for closely-spaced modes. It is shown that the EFD can yield decomposition results for the closely-spaced modes within high accuracy and consistency and its decomposition results compare better than other decomposition methods. In addition, it is shown that the EFD can yield accurate TFR of non-stationary signals. Comparisons between computation times by the EFD, EWT, FDM, VMD and EMD show that the EFD is the most computationally efficient. A future work can be an investigation of applicability the EFD to signals/data of higher dimensions, such as digital images.

A MATLAB implementation of the proposed algorithm will be available at the MATLAB Central.

Acknowledgments

The authors gratefully acknowledge valuable discussions with and input from Dr. Gang Yu, Dr. Pushpendra Singh, Dr. Shiqian Chen and Dr. Heng Li. They also thank the people who share their contributions to the signal processing community.

Conflicts of Interest: The authors declare no conflict of interest.

References

- [1] A. Bhattacharyya, R.B. Pachori, A Multivariate Approach for Patient-Specific EEG Seizure Detection Using Empirical Wavelet Transform, *IEEE Trans. Biomed. Eng.* 64 (2017) 2003–2015. <https://doi.org/10.1109/TBME.2017.2650259>.
- [2] F. Li, B. Zhang, S. Verma, K.J. Marfurt, Seismic signal denoising using thresholded variational mode decomposition, *Explor. Geophys.* 49 (2017) 450–461. <https://doi.org/10.1071/EG17004>.
- [3] J. Pan, J. Chen, Y. Zi, Y. Li, Z. He, Mono-component feature extraction for mechanical fault diagnosis using modified empirical wavelet transform via data-driven adaptive Fourier spectrum segment, *Mech. Syst. Signal Process.* 72–73 (2016) 160–183. <https://doi.org/10.1016/j.ymssp.2015.10.017>.
- [4] S. Chen, Y. Yang, Z. Peng, X. Dong, W. Zhang, G. Meng, Adaptive chirp mode pursuit: Algorithm and applications, *Mech. Syst. Signal Process.* 116 (2019) 566–584. <https://doi.org/10.1016/j.ymssp.2018.06.052>.
- [5] A. Upadhyay, R.B. Pachori, Speech enhancement based on mEMD-VMD method, *Electron. Lett.* 53 (2017) 502–504. <https://doi.org/10.1049/el.2016.4439>.
- [6] D. Iatsenko, P.V.E. McClintock, A. Stefanovska, Nonlinear mode decomposition: A noise-robust, adaptive decomposition method, *Phys. Rev. E - Stat. Nonlinear, Soft Matter Phys.* 92 (2015) 1–25. <https://doi.org/10.1103/PhysRevE.92.032916>.
- [7] H.H.L. N.E. Huang, Z. Shen, S.R. Long, M.C. Wu, H.H. Shih, Q. Zheng, N.C. Yen, C.C. Tung, The empirical mode decomposition and the Hilbert spectrum for nonlinear and non-stationary time series analysis, *Proc. R. Soc. London. Ser. A Math. Phys. Eng. Sci.* 454 (1998) 903–995. <https://doi.org/10.1098/rspa.1998.0193>.
- [8] G. Rilling, P. Flandrin, P. Goncalves, On empirical mode decomposition and its algorithms, *IEEE-EURASIP Work. Nonlinear Signal Image Process.* 3 (2003) 8–11.
- [9] R.T. Rato, M.D. Ortigueira, A.G. Batista, On the HHT, its problems, and some solutions, *Mech. Syst. Signal Process.* 22 (2008) 1374–1394. <https://doi.org/10.1016/j.ymssp.2007.11.028>.
- [10] Z. Wu, N.E. Huang, Ensemble empirical mode decomposition: A noise-assisted data analysis method, *Adv. Adapt. Data Anal.* 1 (2009) 1–41.

<https://doi.org/10.1142/S1793536909000047>.

[11]M.E. Torres, M.A. Colominas, G. Schlotthauer, P. Flandrin, A complete ensemble empirical mode decomposition with adaptive noise, in: ICASSP, IEEE Int. Conf. Acoust. Speech Signal Process. - Proc., IEEE, 2011: pp. 4144–4147. <https://doi.org/10.1109/ICASSP.2011.5947265>.

[12]H. Li, Z. Li, W. Mo, A time varying filter approach for empirical mode decomposition, *Signal Processing*. 138 (2017) 146–158. <https://doi.org/10.1016/j.sigpro.2017.03.019>.

[13]K. Dragomiretskiy, D. Zosso, Variational mode decomposition, *IEEE Trans. Signal Process.* 62 (2014) 531–544. <https://doi.org/10.1109/TSP.2013.2288675>.

[14]S.I. McNeill, Decomposing a signal into short-time narrow-banded modes, *J. Sound Vib.* 373 (2016) 325–339. <https://doi.org/10.1016/j.jsv.2016.03.015>.

[15]S. Chen, X. Dong, Z. Peng, W. Zhang, G. Meng, Nonlinear chirp mode decomposition: A variational method, *IEEE Trans. Signal Process.* 65 (2017) 6024–6037. <https://doi.org/10.1109/TSP.2017.2731300>.

[16]J. Gilles, Empirical wavelet transform, *IEEE Trans. Signal Process.* 61 (2013) 3999–4010. <https://doi.org/10.1109/TSP.2013.2265222>.

[17]Z. Luo, T. Liu, S. Yan, M. Qian, Revised empirical wavelet transform based on autoregressive power spectrum and its application to the mode decomposition of deployable structure, *J. Sound Vib.* 431 (2018) 70–87. <https://doi.org/10.1016/j.jsv.2018.06.001>.

[18]Y. Xin, H. Hao, J. Li, Operational modal identification of structures based on improved empirical wavelet transform, *Struct. Control Heal. Monit.* 26 (2019) 1–21. <https://doi.org/10.1002/stc.2323>.

[19]J.P. Amezquita-Sanchez, H. Adeli, A new music-empirical wavelet transform methodology for time-frequency analysis of noisy nonlinear and non-stationary signals, *Digit. Signal Process. A Rev. J.* 45 (2015) 55–68. <https://doi.org/10.1016/j.dsp.2015.06.013>.

[20]P. Singh, S.D. Joshi, R.K. Patney, K. Saha, The Fourier decomposition method for nonlinear and non-stationary time series analysis, *Proc. R. Soc. A Math. Phys. Eng. Sci.* 473 (2017). <https://doi.org/10.1098/rspa.2016.0871>.

[21]A. V Oppenheim, A.S. Willsky, W.S. Hamid, *Signals and Systems* (2nd Edition), (1996).

[22]I. Daubechies, Ten lectures on wavelets, in: *CBMS-NSF Reg. Conf. Ser. Appl. Math.*,

Society for Industrial and Applied Mathematics, Philadelphia, 1992: pp. 198–202.

[23]J. Gilles, G. Tran, S. Osher, 2D Empirical Transforms. Wavelets, Ridgelets, and Curvelets Revisited, *SIAM J. Imaging Sci.* 7 (2014) 157–186. <https://doi.org/10.1137/130923774>.

[24]B. Picinbono, On instantaneous amplitude and phase of signals, *IEEE Trans. Signal Process.* 45 (1997) 552–560. <https://doi.org/10.1109/78.558469>.

[25]F.J. Harris, *Multirate signal processing for communication systems*, Prentice Hall PTR, 2004.

[26]T.Y. Hou, Z. Shi, Adaptive data analysis via sparse time-frequency representation, *Adv. Adapt. Data Anal.* 3 (2011) 1–28. <https://doi.org/10.1142/S1793536911000647>.

[27]G. Rilling, P. Flandrin, One or Two Frequencies? The Empirical Mode Decomposition Answers, *IEEE Trans. Signal Process.* 56 (2008) 85–95.